An ENDOR analysis of a diatomic sulphur defect in RbI

An ENDOR analysis of a diatomic sulphur defect in RbI

S Van Doorslaer, F Callens, F Maes and P Matthys

Laboratory for Crystallography and Study of the Solid State, Krijgslaan 281-S1, B-9000 Gent, Belgium

Abstract. In this article, an ENDOR analysis of the S_2^- defect in RbI is presented. A complete angular variation of one set of ^{85}Rb and ^{87}Rb ENDOR transitions is measured. The corresponding hyperfine and nuclear quadrupole coupling tensors are determined. The orientation of the principal axes of these tensors is in good agreement with the overall D_{2h} symmetry of the S_2^- ion in the lattice. The ENDOR results clearly lead to a monovacancy model, wherein the S_2^- ion is replacing one I^- ion on a lattice site. The linewidth of the EPR signals can be explained using the ENDOR data. A comparison with previous ENDOR studies of O_2^- and S_2^- defects in rubidium halides is made.

1. Introduction

EPR studies of X_2^- defects (X = O, S and Se) in alkali halide single crystals [1–12] could not always reveal unambiguously the defect structure. Depending on the lattice, the paramagnetic p lobes of the X_2^- defect may be oriented along a $[\bar{1}10]$ or a [001] direction. Problems arose when in KCl two S_2^- molecular ions with differing p-lobe orientations were identified in the same single-crystal sample. The monovacancy model was subsequently questioned and in some cases a divacancy model (in which X_2^- replaces two adjacent halide ions) was considered.

To solve the structural problems, ENDOR investigations were started on a whole series of X_2^- defects (X = O, S, Se) in different alkali halides. The ENDOR results for S_2^- in RbCl [13] and O_2^- in RbCl [14] and RbI [15] clearly led to a monovacancy model. In this paper, an ENDOR study of an S_2^- defect in RbI is presented. A comparison with the earlier ENDOR studies is made.

2. Experimental techniques

The single crystal was grown by the Bridgman method. The RbI powder (Merck) was mixed with 0.15 wt% S (UCB) and 0.1 wt% Rb (Merck). Samples thus grown were routinely quenched from 600 °C to room temperature (RT), though this treatment did not affect the S_2^- spectra reported below. The crystals were irradiated at RT for typically half an hour with a tungsten anticathode Philips x-ray tube, operated at 60 kV and 40 mA.

The EPR spectra were recorded using a Bruker ESP300 X-band spectrometer, with maximum microwave power of 200 mW. The optimal detection conditions were 25 K and 100 mW microwave power.

The ENDOR spectra were recorded on the same spectrometer, equipped with a Bruker ESP 353E ENDOR/Triple extension (an EN374 RF amplifier with a maximum power of

200 W and an EN 525 Schomandl synthesizer). The best detection conditions were 6 K and 100 mW microwave power at maximum RF power. The detection temperature was found to be crucial. The RF was modulated at 12.5 kHz with a modulation depth of 100 kHz.

3. Results

3.1. EPR results

Vannotti and Morton [4] first detected the S_2^- ion in RbI with EPR. The orthorhombic centre was found to have the following g-tensor : $g_x = 1.2895(4)$, $g_y = 1.2968(4)$ and $g_z = 3.3595(4)$. The number in brackets indicates the error in the last digit. The x-, y- and z-axes correspond to the $[\bar{1}10]$, $[001]$ and $[110]$ directions. No superhyperfine interaction could be resolved in the EPR spectra. Vannotti and Morton [4], in accordance with [2], showed that the largest g-value corresponds to the direction of the molecular axis. The smallest g-value is found to determine the axis of the paramagnetic p lobes (here, the g_x-direction).

3.2. ENDOR results

3.2.1. ENDOR spectra corresponding to Rb superhyperfine interaction 1. For both Rb isotopes, the ENDOR angular variations are measured in the g_x–g_z-plane (plane 1, $B_0 \perp [001]$) and in the plane containing the g_y-direction ($B_0 \perp [100]$ or $B_0 \perp [010]$, plane 2). The natural abundance of ^{85}Rb and ^{87}Rb (73.27% and 27.83%, respectively) is reflected in the line intensity of the ENDOR signals. As an example, figure 1 shows the ^{85}Rb ENDOR angular variation in plane 1. Figure 2 shows the ENDOR spectra for $B_0 \parallel [001]$ axis (plane 2).

The spectra were analysed using the standard Hamiltonian for a single nucleus ($I > 1/2$) coupled with an unpaired electron ($S = 1/2$)

$$\hat{\mathcal{H}} = \beta \hat{S}^T \mathbf{g} B + \hat{I}^T \mathbf{A} \hat{S} - \beta_N \hat{I}^T \mathbf{g}_N B + \hat{I}^T \mathbf{Q} \hat{I}. \tag{1}$$

The ENDOR frequencies were analysed by complete diagonalization of the spin-Hamiltonian matrix. The resulting principal values and corresponding axes of the hyperfine tensor and nuclear quadrupole tensor are given in table 1. The theoretical angular variations calculated using the values of table 1 are shown in figure 1 (full lines).

Table 1. Principal values (in MHz) and axes of the ^{85}Rb and ^{87}Rb SHF and nuclear quadrupole tensor for RbI:S_2^-. The numbers in brackets reflect the errors in the last digits.

| | ^{85}Rb | ^{87}Rb | Angles with respect to | | |
			g_x	g_y	g_z
A_x	19.87(1)	67.34(1)	30.7(2)	90	120.7(2)
A_y	12.34(1)	41.81(1)	90	0	90
A_z	10.46(1)	35.45(1)	−59.3(2)	90	30.7(2)
Q_x	0.16(1)	0.25(1)	23.3(2)	90	113.3(2)
Q_y	0.09(1)	0.15(1)	90	0	90
Q_z	−0.25(1)	−0.40(1)	−66.7(2)	90	23.3(2)

The **A** tensor is nearly axial. The direction of the largest Q-value is found to be 23.3° tilted away from the g_z-axis.
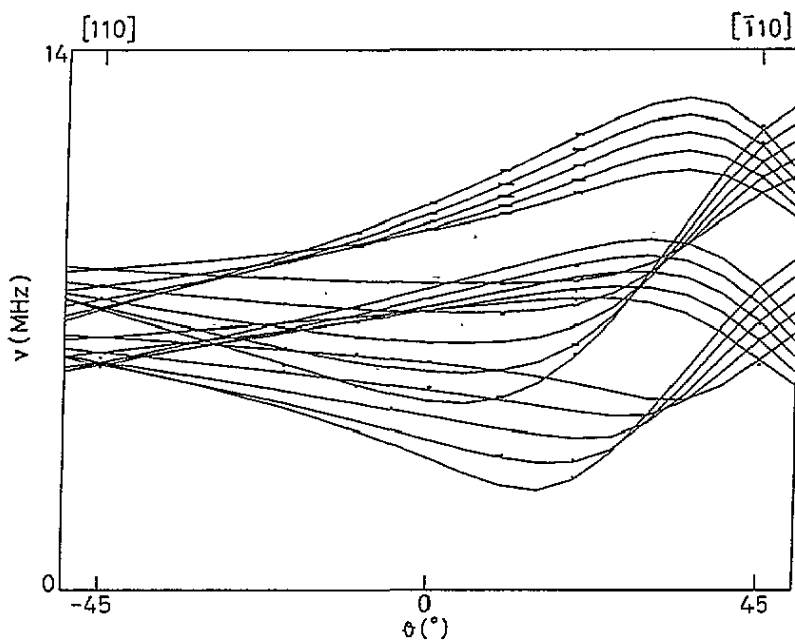
Figure 1. The angular variation of the ^{85}Rb ENDOR transitions in plane 1. The rectangles show the experimental ENDOR positions; the full lines indicate the theoretical angular variation calculated using the values of table 1.
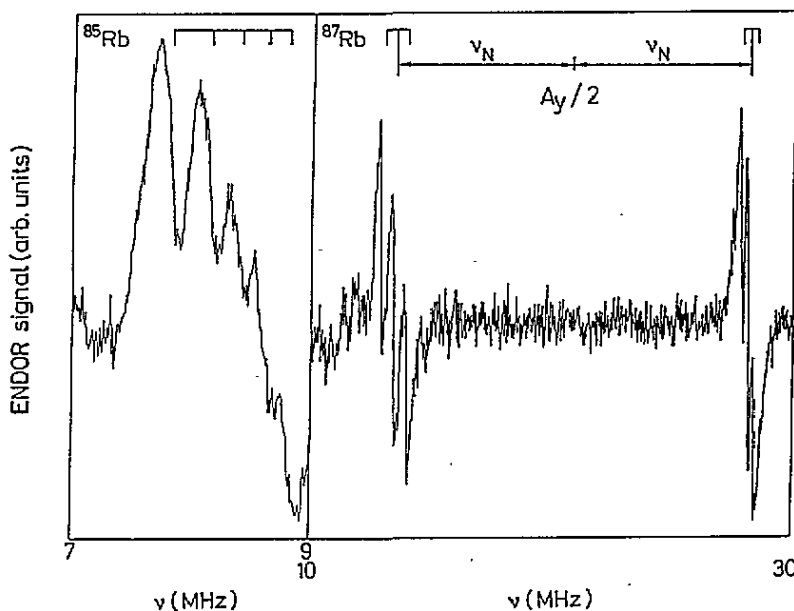

Figure 2. A typical ENDOR spectrum for $B_0 \parallel [001]$ axes. The ^{85}Rb and ^{87}Rb lines are indicated.

4. Discussion

In this discussion, it will be shown that the ENDOR features are consistent with a monovacancy model in which the S_2^- ion is replacing a single I^- ion on a lattice site.

The observed Rb superhyperfine (SHF) interaction is due to the four nearest-neighbouring Rb ions in the (001) plane (figure 3, A1). The discussion will be for the ^{85}Rb SHF interaction unless mentioned otherwise. All results can be converted for the ^{87}Rb SHF interaction.
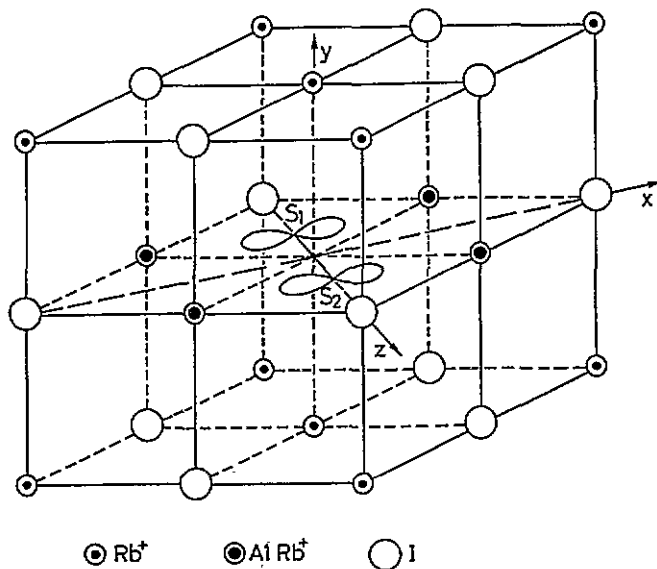

Figure 3. The monovacancy model for the S_2^- defect in RbI. The Rb nuclei labelled A1 cause interaction 1.

4.1. The superhyperfine tensor

The analysis of the spin-Hamiltonian parameters obtained was done in the same way as for the O_2^- defect in RbCl and RbI [12, 14]. Again, the SHF interaction could be described considering both covalency effects and point dipolar contributions. For the latter contribution, the formulas derived by Hurst *et al* [16] were used. In order to account for the covalency, Shuey and Zeller [3] derived expressions for the SHF components assuming the wavefunction of the unpaired electron in the neighbourhood of the Rb nucleus to be

$$|\psi_\pm\rangle = (\cos\,\alpha)(c_\sigma\phi_\sigma + c_s\phi_s)|\pm\tfrac{1}{2}\rangle \pm i(\sin\,\alpha)c_\pi\phi_\pi|\pm\tfrac{1}{2}\rangle \qquad (2)$$

in which

$$\phi_\sigma = -(4p)_x\cos\delta + (4p)_z\sin\delta \qquad \phi_\pi = (4p)_y \qquad \phi_s = (4s) \qquad (3)$$

and δ is the angle between the g_x-axis and the ϕ_σ-lobe (see figure 4). $|\pm 1/2\rangle$ are the eigenstates of $\hat{S}_z$, and $\tan(2\alpha) = \lambda/\Delta$, where Δ is a crystal-field parameter and λ is the positive spin–orbit coupling constant. For the RbI:S_2^- case, Vannotti and Morton [4] found that $\lambda/\Delta = 1.20$ and $\alpha = 25°$. To a first approximation, the ϕ_σ-lobe is expected along an axis connecting the Rb nucleus and the nearest S atom. Using a S–S distance of 0.189 nm [17], and the Rb–I distance 0.368 nm, the value for δ is found to be 32.3°.

Using $\delta = 32.3°$, it was not possible to fit the hyperfine values exactly. However, when varying the δ-value to 35.6° ($\pm 0.5°$), the theory could be fitted perfectly to the experiment. The change in δ is physically acceptable (see figure 4). After all, the ϕ_σ-lobe was only in a first approximation taken to be pointing to the nearest S atom. r was found to be 0.366 nm, which is approximately the lattice distance. In table 2 the coefficients c_s^2, c_σ^2
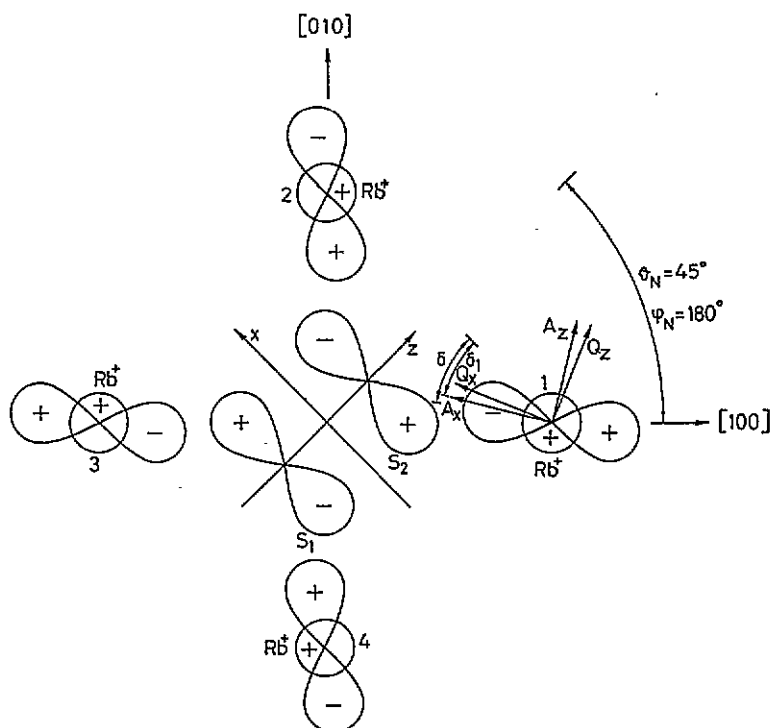
Figure 4. The orientation of the principal axes of the Rb SHF and nuclear quadrupole tensors. δ is the angle between the g_x-axis and the ϕ_σ-lobe; δ_1 is the angle between the A_x-axis and the g_x-axis.

Table 2. A comparison between the calculated coefficients c_s^2, c_σ^2 and c_π^2 obtained from the ENDOR results for RbI:S_2^-, RbCl:S_2^- [13], RbI:O_2^- [15] and RbCl:O_2^- [14], taking into account that for Rb we have $|\Psi(0)|_{4s}^2 = 29.28$ au and $\langle r^{-3}\rangle_{4p} = 20.24$ au [18]. (The number in brackets indicates the error in the last digit).

	c_s^2	c_σ^2	c_π^2
RbI:S_2^-	0.001 44(1)	0.005 32(1)	0.000 68(5)
RbCl:S_2^-	0.002 14(1)	0.009 79(1)	0.000 59(5)
RbI:O_2^-	0.000 41(1)	0.002 02(1)	0.000 38(5)
RbCl:O_2^-	0.000 65(1)	0.003 30(1)	0.000 58(5)

and c_π^2 are given. Comparison with earlier results reveals interesting features. Table 2 shows that when going from RbCl to RbI the values of c_s^2 and c_π^2 decrease for both the O_2^- and the S_2^- defect in approximately the same way as the $1/a^3$-values (with a the lattice constant, $a(\text{RbCl}) = 0.328$ nm, $a(\text{RbI}) = 0.368$ nm). Apparently, the dominant feature for these coefficients is the change of the lattice. We have to keep in mind, however, that the spin densities in the ϕ_s-, ϕ_σ- and ϕ_π-orbitals are determined by $(\cos^2 \alpha)c_s^2$, $(\cos^2 \alpha)c_\sigma^2$ and $(\sin^2 \alpha)c_\pi^2$, respectively, rather than simply by c_s^2, c_σ^2 and c_π^2. Furthermore the use of (2) may be in principle criticized since assuming the weighing factors $\cos \alpha$ and $\sin \alpha$ for, respectively, the Γ_2^+ and Γ_4^+ contributions on the Rb nuclei implies, among other things, that the spin–orbit coupling constants are the same at the S_2^- as at the Rb^+ location. In practice, however, the value of $\cos^2 \alpha$ is so close to 1 that the conclusions for c_s^2 and c_σ^2

will be hardly affected. The c_π^2-values are much less reliable because they are small and strongly influenced by errors in $\sin^2 \alpha$, c_σ^2 and δ. As a result the trend is not so obvious when comparing the four radicals in table 2.

The ENDOR results can be related to the EPR linewidths in the following way. Up to first order the values of the SHF splitting K in the EPR spectra are defined as [19]

$$B_0 \parallel g_x\text{-axis}: \quad K(10^{-4}\ \text{T}) = \frac{\sqrt{A_{xx}^2 + A_{zx}^2}}{\beta g_x}$$

$$B_0 \parallel g_y\text{-axis}: \quad K(10^{-4}\ \text{T}) = \frac{A_{yy}}{\beta g_y} \tag{4}$$

$$B_0 \parallel g_z\text{-axis}: \quad K(10^{-4}\ \text{T}) = \frac{\sqrt{A_{zz}^2 + A_{xz}^2}}{\beta g_z}$$

in which the **A** matrix elements are given in MHz.

Table 3. Superhyperfine splittings K (in 10^{-4} T) for some specific directions of the magnetic field, calculated using the ENDOR results. The numbers in brackets indicate the error in the last digit.

	^{85}Rb	^{87}Rb
$K(B_0 \parallel [\bar{1}10])$	9.91(2)	33.58(2)
$K(B_0 \parallel [001])$	6.80(1)	23.00(1)
$K(B_0 \parallel [110])$	2.88(2)	9.76(2)

The values of the ^{85}Rb and ^{87}Rb splittings for these specific directions of the magnetic field are given in table 3.

Table 4. A comparison between the EPR linewidths (in 10^{-4} T) obtained from the ENDOR results (a) and those obtained experimentally by Vannotti and Morton [4] (b).

$B_0 \parallel$	ΔB (a)†	ΔB (b)†
$[\bar{1}10]$	99	105
$[001]$	77	91
$[110]$	40	33

† With an error of 5%.

The simulation of the resulting EPR line is complicated by the presence of the two isotopes with different natural abundances and the fact that four equivalent Rb ions contribute to the observed interaction. Assuming that each SHF line has a homogeneous linewidth of about 10×10^{-4} T, we could simulate the resulting EPR signals with an unresolved SHF structure. The EPR linewidths are given in table 4 and compared to the ones obtained experimentally by Vannotti and Morton [4]. The rather large error in the theoretical linewidths is due to the fact that the homogeneous linewidth of the SHF signals can be chosen arbitrarily. The observed linewidths are governed by the SHF interaction with the four nearest-neighbour Rb nuclei.

4.2. The nuclear quadrupole tensor

As a rule of thumb, the **Q** tensor should have the same symmetry as the **A** tensor, which is the case. Although the tilt angle of the **A** and **Q** tensors does not differ much, it is found

that the direction of the largest Q value is near the g_z-axis, which is clearly different from what is found in the RbCl:S_2^- case [13], where the largest Q value was pointing in the direction of the defect.

The Q tensor is determined by a lot of factors: the electric quadrupole moment, the position of the Rb nucleus with respect to the S_2^- ion, the distribution of the unpaired electron over the p lobes of the X_2^- defect and over the lobes of the Rb ion considered, the nuclear spin of Rb, the surrounding ions, and the Sternheimer factor of the cation ($\gamma_\infty(Rb^+) = -47.2$ [20]). In general we can write that

$$\frac{Q_z}{2} = \frac{1}{4\pi\varepsilon_0}\frac{e^2 Q}{2I(2I-1)}\left(\sum_i \frac{q_i}{r_i^3}(1-\gamma_\infty) - \frac{2}{5}f_s\langle r^{-3}\rangle_p\right) \tag{5}$$

in which f_s is the density of the unpaired electron in the cation-interacting p lobe (c_σ^2). In a point charge model, q_i and r_i are the charges of and distances from the surrounding ions. This would lead in our case to a zero contribution for the first term. The second term gives rise to a value of -0.276 MHz for $Q_z(^{85}Rb)$. This is in accordance with what was observed. It does not explain the observed tilt angle however. We should keep in mind though that (5) is only a rough estimation. When the unpaired electron belongs to an atom or molecule, the first term of (5) must be integrated over the wavefunction. For atoms, the calculation parallels that of the magnetic dipolar coupling. For a many-electron system, a summation over all electrons should be considered.

For our specific case, the axial symmetry is broken, because of this summation. Moreover, such an anisotropic effect also gives rise to a tilt of the Q tensor axes. The tilt depends on the specific values of the tensor components and is therefore not the same for the different cases studied here.

5. Conclusion

The ENDOR spectra of RbI:S_2^- can be explained when the S_2^- ion is assumed to replace one I^- ion. One set of ^{85}Rb and ^{87}Rb hyperfine and quadrupole interactions could be resolved and ascribed to the nearest-neighbouring Rb ion in the (001) plane. A comparison was made with earlier studies of O_2^- in RbCl and RbI and S_2^- in RbCl. Finally, the linewidths of the EPR signals were explained on the basis of the ENDOR data.

Acknowledgments

References

[1] Känzig W and Cohen M H 1959 *Phys. Rev. Lett.* **3** 509
[2] Zeller H R and Känzig W 1967 *Helv. Phys. Acta* **40** 845
[3] Shuey R T and Zeller H R 1967 *Helv. Phys. Acta* **40** 873
[4] Vannotti L E and Morton J R 1967 *Phys. Rev.* **161** 282
[5] Vannotti L E and Morton J R 1967 *Phys. Lett.* **24A** 250
[6] Matthys P, Callens F and Boesman E 1983 *Solid State Commun.* **45** 1
[7] Callens R, Callens F, Matthys P and Boesman E 1988 *Phys. Status Solidi* b **148** 683
[8] Callens F, Maes F, Matthys P and Boesman E 1989 *J. Phys.: Condens. Matter* **1** 6912
[9] Maes F, Callens F, Matthys P and Boesman E 1990 *J. Phys. Chem. Solids* **51** 1289

[10] Maes F, Callens F, Matthys P and Boesman E 1990 *Phys. Status Solidi* b **161** K1

[11] Maes F, Matthys P, Callens F and Boesman E 1991 *Solid State Commun.* **80** 583

[12] Maes F, Matthys P, Callens F, Moens P and Boesman E 1992 *J. Phys.: Condens. Matter* 4 249

[13] Van Doorslaer S, Maes F, Callens F, Moens P and Boesman E 1994 *J. Chem. Soc. Faraday Trans.* **90** 2541

[14] Van Doorslaer S, Callens F, Maes F and Boesman E 1995 *Phys. Rev.* B **51** 12480

[15] Van Doorslaer S, Callens F, Maes F and Matthys P 1995 *J. Phys.: Condens. Matter* **7** 1909

[16] Hurst G C, Henderson T A and Kreilick R W 1985 *J. Am. Chem. Soc.* **107** 7294

[17] Sutton L E (ed) 1958 *Tables of Interatomic Distances and Configurations in Molecules and Ions* (London : The Chemical Society) p M69

[18] Koh A and Miller D J 1985 *At. Data Nucl. Data Tables* **33** 235

[19] Iwasaki M 1974 *J. Magn. Reson.* **16** 417

[20] Sternheimer R M 1966 *Phys. Rev.* **146** 140